Tunable Electro-Optical and Thermal Optical Modulator Based on a Liquid Crystal-Filled Side Hole Fiber in Fiber Ring Laser

Weihao Lin, Siming Sun, Li-Yang Shao, *Senior Member, IEEE*, Mang I. Vai, *Senior Member, IEEE*, Perry Ping Shum, *Senior Member, IEEE*, Yuhui Liu, and Weizhi Wang

***Abstract*—A new tunable electro-optical and thermal-optical modulator based on a liquid crystal (LC) filled side hole fiber (SHF) in fiber ring laser (FRL) system has been proposed and experimentally demonstrated. The LC is penetrated into the air hole of SHF, and the refractive index (RI) of LC will be altered when an external electrical field or temperature difference is applied due to thermal-optical effects and electro-optic effects. SHF is used as both a filter and a sensing head in the laser cavity. Besides, the resonance wavelength is more sensitive to the temperature variations due to high thermal-optic coefficient when incident light interacts with the internal infiltrated LC. Meanwhile, the sensor has good performance with a high extinction ratio (>42 dB) and a narrow 3-dB bandwidth (less than 0.08 nm). The consequent thermal and electronic sensitivity are measured to be −4.23 nm/°C and 0.604nm/V, respectively. Moreover, the excellent and reliable performance expected to monitor the temperature and electric field as the wavelength-tunable electro-optical devices within a small temperature change range is needed.**

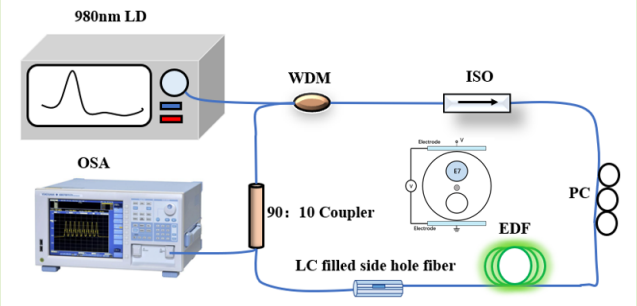

***Index Terms*—Electro-optical modulator, thermal optical modulator, fiber ring laser sensor.**

I. Introduction

OVER the past few years, optical fiber modulator, typically side hole fiber (SHF) based modulator have drawn a great deal of attention due to their high sensibility, low cost, compact size and immunity to electromagnetic interference [1]–[3]. Various fiber-optic modulators are designed to measure magnetic fields [4], electric fields [5], temperature [6], acousto-optic [7], etc., in the power industry, biology, environmental sustainability, and medical systems. Among them, modulation methods based on liquid crystal filling, such as Fabry-Perot interferometer [8], adjustable Sagnac filter [9], [10], tilted fiber grating [11], side hole fiber [12], whispering gallery mode micro-resonator [13], [14] and photonic crystal fiber (PCF) [15]–[17], have been widely studied in thermo-optic and electro-optic modulation.

Nevertheless, the electric field and temperature modulator based on the traditional super-continuous broadband light source (SBS) have disadvantages such as low extinction ratio, low intensity, wide 3dB bandwidth, etc., which limit its application. Eric studied the effect of filler metal on the birefringence optical properties of integrated electrode photonic crystal fiber [18]. M. Fokine proposed an Integrated fiber Mach–Zehnder interferometer for electro-optic switching [19]. At present, the combination of fiber ring laser and fiber modulator is a good solution in the sensing field [20]. The inherent characteristics of fiber laser are high signal-to-noise ratio, peak light intensity and narrow 3dB bandwidth, thus improving the sensitivity and detection accuracy. Lin *et al.* demonstrated a FRL sensor with Er doped fiber peanut structure to detect refractive index and temperature.

Manuscript received September 29, 2021; revised October 18, 2021; accepted October 22, 2021. Date of publication October 29, 2021; date of current version December 14, 2021. This work was supported in part by the Startup Fund from Southern University of Science and Technology, in part by the Project Future Greater-Bay Area Network Facilities for Large-Scale Experiments and Applications under Grant LZC0019, and in part by The Verification Platform of Multitier Coverage Communication Network for Oceans under Grant LZC0020. The associate editor coordinating the review of this article and approving it for publication was Prof. Arnaldo G. Leal-Junior. *(Corresponding author: Li-Yang Shao.)*

Weihao Lin, Siming Sun, Perry Ping Shum, and Yuhui Liu are with the Department of Electrical and Electronic Engineering, Southern University of Science and Technology, Shenzhen 518005, China (e-mail: 11510630@mail.sustech.edu.cn; shenp@sustech.edu.cn; liuyh@mail.sustech.edu.cn).

Li-Yang Shao is with the Department of Electrical and Electronic Engineering, Southern University of Science and Technology, Shenzhen 518055, China, and also with the Peng Cheng Laboratory, Shenzhen 518005, China (e-mail: shaoly@sustech.edu.cn).

Mang I. Vai is with the Department of Electrical and Computer Engineering, Faculty of Science and Technology, University of Macau, Macau, China (e-mail: fstmiv@um.edu.mo).

Weizhi Wang is with the Peng Cheng Laboratory, Shenzhen, Guangdong 518055, China (e-mail: wangwzh@pcl.ac.cn).

Digital Object Identifier 10.1109/JSEN.2021.3124220

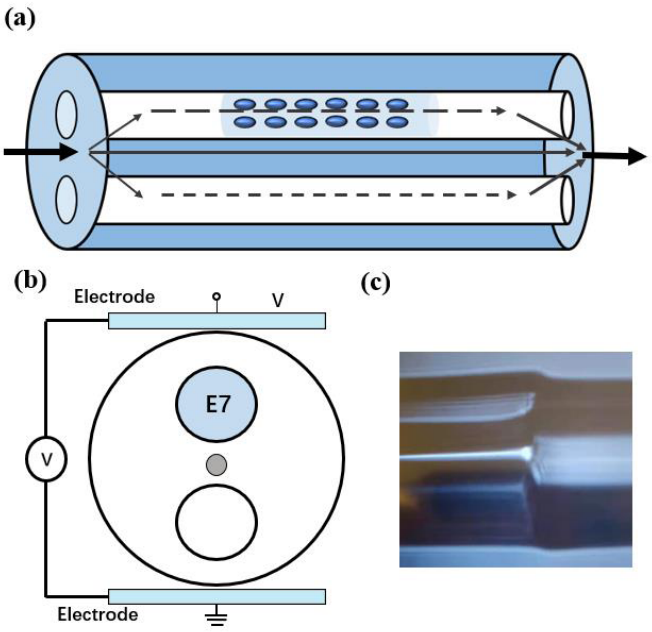

Fig. 1. (a) The schematic diagram of the LC-SHF structure (b) Cross section of the designed SHF (c) photography of the fabricated device.

The temperature sensitivity is 0.158 nm/°C without using additional filters [21]. Tapered fibers filled with isopropanol [22] and cascaded Sagnac rings [23] are also designed for temperature modulation. The sensitivities are 4.031 nm/°C and 1.92 nm/°C, respectively.

The novel Electro-Optical and Thermal Optical Modulator presented here comprises a SHF, whose effective refractive index varies with the temperature and external electric field intensity. The modulator is manufactured by filling one of the edge holes of the SHF with a commercial E7 LC (Suzhou King Optronics Co., Ltd., China). Because of thermal-optical effect and electro-optic effect, the interference of core mode and cladded mode appears in LC-SHF. Under the interference effect, LC will shift its wavelength when the electric field and temperature change. The experimental results show that the emission wavelength of the fiber ring laser is blue shifted with the increase of temperature, and the sensitivity is 4.23 nm/°C, respectively. Resonance wavelengths can be electrically tuned from 1530nm to more than 1560nm, with an average sensitivity of 0.604nm/ V_{rms}. In addition, compared with the traditional electro-optic modulator, the proposed thermo-optic and electro-optic modulator based on fiber laser cavity has the advantages of high intensity, high optical signal-to-noise ratio, narrow band and so on, and has great application potential in remote electric field and temperature measurement.

II. Experimental Setup and Principle

The schematic diagram of the device is shown in Fig. 1(a) and (b). The designed SHF consists of a fiber core and two air holes, with a pore diameter of 40 μm and a pore spacing of 200 μm. The cladding diameter of SHF is 5 μm mismatch the cladding diameter of standard single-mode fiber which leads to interference between modes. The SHF was

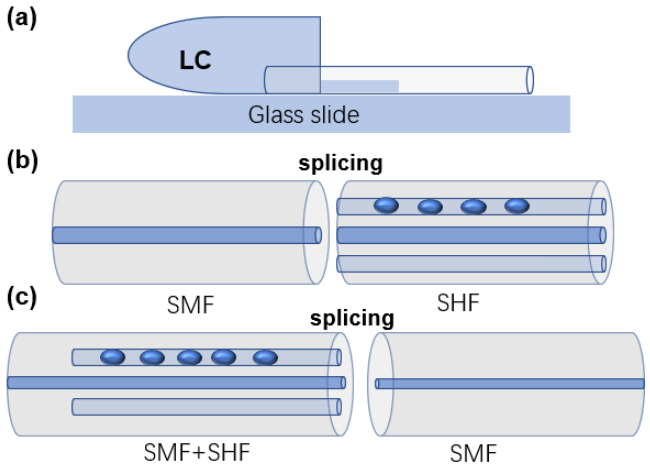

Fig. 2. Fabrication process of the infiltrated liquid crystal single mode fiber-side hole fiber-single mode fiber MZI electric field sensor.

not fully filled with LC, and the air core of the two splicing points were spliced into Mach-Zehnder interferometer (MZI). To selectively fill the unilateral stomata with liquid crystals. We glued a small amount of UV glue to an air hole in the SHF by manually driving the motor of the fuse adapter (FSM-60s Fujikura, Tokyo, Japan). Finally, the glue curing operation is carried out. At this time, only one pore of SHF remains open, and the liquid crystal can be easily filled to the unblocked pore of SHF through capillary effect. Optical fiber devices based on MZI belong to optical phase modulation type. When the external temperature or electric field changes, the phase of the transmitted light also changes. By using MZI technology, the phase change can be transformed into the wavelength change, and the corresponding physical quantity can be detected. The photograph of the assembly is shown in Fig.1 (c). In order to avoid the collapse of pores during welding. Before performing the welding operation, the welding program of the welding machine (Fujikura, FSM-60S, Japan) must be edited to optimize the discharge time to 400ms and the discharge power to the standard 45bit. At the same time, avoid the vibration of the side hole optical fiber filled with liquid crystal, which may overflow to the flat end of the optical fiber.

In the experiment, SHF was inserted into a glass slide with liquid crystal droplets. Due to capillary action, PCF can be filled with liquid crystal in a very short time as shown in fig.2(a). Apply a small amount of UV glue on the single-mode fiber, and then put it into the fusion splicer. Move the SHF by manually driving the welding machine, and then offset the fiber by a certain distance to ensure that the single-mode fiber is aligned with only one air hole on the left SHF. Glue one of the air holes with the glue of the air hole to ensure that the other air hole is not stuck as shown in fig.2(b) and (c).

As shown in Fig. 3(a) and Fig. 3(b), the LC-SHF used for the sensor is a liquid crystal cell made of indium tin oxide (ITO) conductive glass (thickness 1.05 mm). Before LC injection, conductive grade is placed on both sides of ITO glass to fix the initial orientation of liquid crystal. A variable AC voltage source load is applied to the SHF-coated ITO glass. If the switch is off, no voltage is applied and

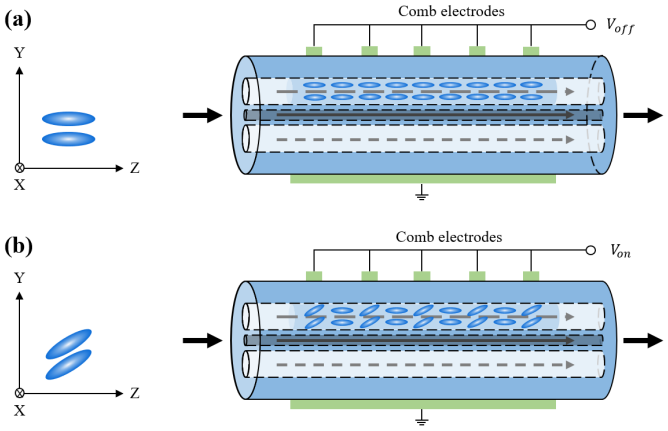

Fig. 3. (a) When the liquid crystal molecule is grounded, the LC molecule is parallel to the optical axis; (b) LC molecules rotate under an electric field when the liquid crystal molecules are electrified.

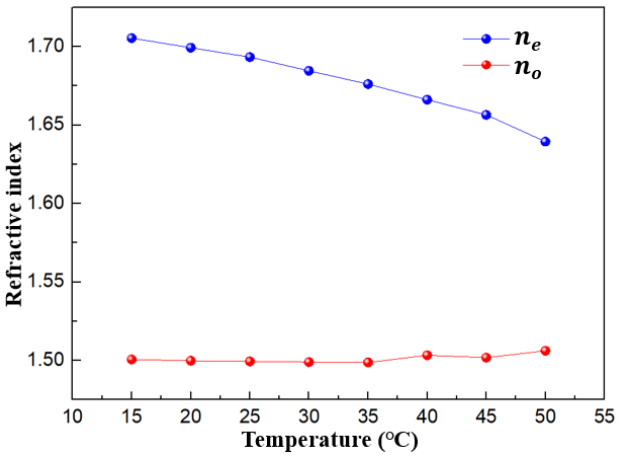

Fig. 4. Thermal-optic characteristics of E7 in the temperature range of 15 °C to 50 °C.

the LC molecules are parallel to the optical axis. But if the switch is turned on, the LC molecules are rotated by an electric field and the effective core refractive index is modulated regularly. Similarly, when the ambient temperature is changed, the effective refractive index is modulated by the thermo-optical effect of the liquid crystal to change the orientation of LC molecules. According to the principle of SHF, the coupling core mode and cladding mode satisfying the phase matching condition are determined, that is, the resonant wavelength is determined.

The output light of the intensity interference spectrum can be expressed by the following equation [24]:

$$I = I_1 + I_2 + 2\sqrt{I_1 I_2} COS\left[2\pi L\left(n_{eff}^{cl} - \frac{n_{cm,n}^{eff}}{\lambda}\right)\right] \quad (1)$$

where I is the intensity of the total interference intensity, I_1 and I_2 are the intensity of the core and cladding modes, respectively. Where λ is the wavelength of the transmitted light, L is the interference length, n_{eff}^{cl} is the effective refractive index of the core mode, $n_{cm,n}^{eff}$ is the effective refractive index of the J-order cladding mode. When the optical pass is modulated by the modulator, the difference between the cladding mode and the core mode can be expressed as [21]:

$$\Delta\varphi = 2\pi L\left(n_{cl}^{eff} - n_{cm,n}^{eff}\right)\Big/\lambda \quad (2)$$

$$\lambda_{dip} = 2L\left(n_{cl}^{eff} - n_{cm,n}^{eff}\right)\Big/(2m+1) \quad (3)$$

Under the influence of thermal-optical effect, when the temperature changes, the RI of LC filled in the SHF micropores will change significantly, so the mode relative refractive index between the fiber core and cladding will change correspondingly. The change of effective refractive index is shown in Fig.4. The relationship between RI change of characteristic wavelength and ambient temperature is as follows [25]:

$$\Delta n_{eff}(T) = \Delta n_{eff} + \frac{\partial \Delta n_{eff}}{\partial T}|T = T_0 \Delta T(4) \quad (4)$$

T_0 is the initial temperature. Δn_{eff} changes will result in a shift of λ_{dip}. The displacement of the wavelength due to the temperature change ΔT can be expressed as:

$$\Delta\lambda_{dip}^{m} = \frac{2}{2m+1}\frac{\partial \Delta n_{eff}}{\partial T}\Delta T \cdot L = \lambda_{dip}^{m}\beta\Delta T \quad (5)$$

where β is the effective thermal optical coefficient of LC-SHF.

LC has a Frederick transform threshold E_{th} [21]. When the nematic liquid crystal E7 fills SHF, LC molecules are aligned axially along the pores. The y-axis is set as the direction of the applied electric field, and the x-axis is set along the horizontal direction. The structure diagram is shown in Fig. 2. Then, when LC molecules rotate, they form an angle with the air axis. The relation between the angle of LC molecule and the applied electric field is [25]:

$$\theta = \frac{\pi}{2} - 2tan^{-1}\left[\exp\left(-\frac{E_{eff} - E_{th}}{30E_{th}}\right)\right], \quad E_{eff} > E_{th} \quad (6)$$

where, E_{th} is the threshold electric field dependent on LC properties, and E_{eff} is the effective electric field acting on LC molecules to determine their arrangement. When the electric field is higher than ETH, LC molecules are rearranged along the liquid crystal cell, and the angle changes with the electric field. RI of LC molecule in x and y directions can be expressed as [24]:

$$n_x = n_0 \quad (7)$$

$$n_y = \left(\frac{sin^2(\theta)}{n_e^2} + \frac{cos^2(\theta)}{n_o^2}\right)^{-\frac{1}{2}} \quad (8)$$

where n_o is the ordinary refractive index of LC; n_e is the extraordinary refractive index of LC. The effective RI of LC is expressed as:

$$n_{eff} = \sqrt{\frac{n_y^2 + n_x^2}{3}} \quad (9)$$

Due to the existence of thermal-optical effect, thermal expansion effect and elastic-optical effect, the central wavelength of side-hole fiber will drift with the change of external temperature, and the responsiveness of the resonant wavelength in two polarization directions is different due to the different elastic-optical effect. When the light is incident from

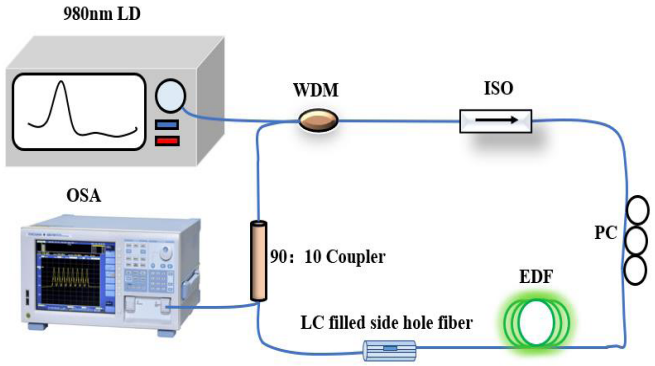

Fig. 5. The intracavity sensing system based on FRL.

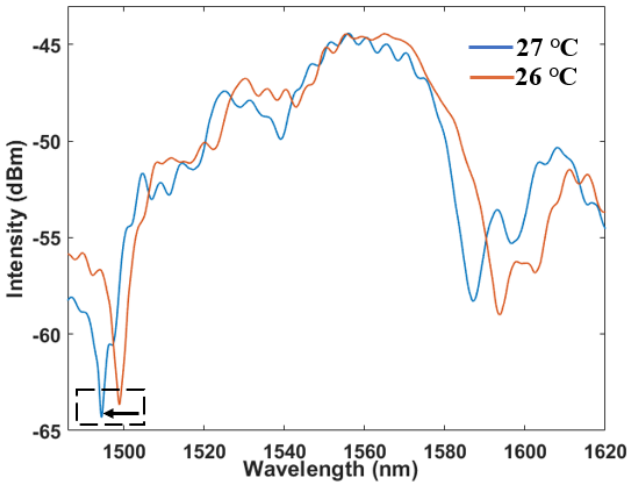

Fig. 6. Transmission spectrum of LC-SHF structure in supercontinuum light source.

the single-mode fiber through the first fusion point between the single-mode fiber and SHF, a part of the core mode excites the cladding mode. The core mode and the excited cladding mode meet and are coupled to the single-mode fiber at the second fusion point between the alcohol-filled SHF and the single-mode fiber. Due to the different effective refractive index of the core and cladding of the LC filled SHF, and the length of the LC filled SHF, the interference occurred at the second fusion point, forming a MZI.

First, the interference spectra of the prepared LC-SHF structure were observed by using a supercontinuum light source and an optical spectral analyzer (OSA, Yokogawa AQ6370D) with a resolution of 0.02 nm. The detection results are shown in Fig.6. The structural diagram of the proposed FRL modulator is shown in Fig. 5. A 980nm laser diode (PL-974-500-FC/APC-P-M) and a 1.6-m erbium-doped fiber (EDF) are connected via a 980/1550nm WDM. The laser diode works as a pump source. The effect of isolators is to suppress unwanted reflections. The light is then transmitted to a 5.5-mm-long SHF filled with the E7 liquid crystal, which is used as both a wavelength selection filter and a sensing head due to clad mode and core mode interference effects. Finally, the output spectrum is connected to the 10:90 coupler,

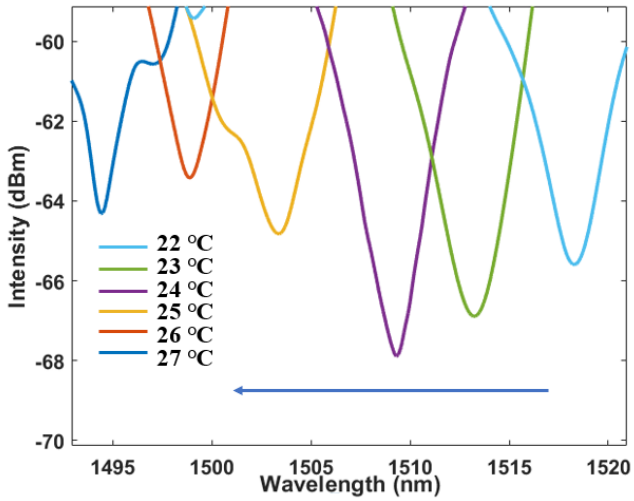

Fig. 7. Transmission spectrum evolution in supercontinuum light source with temperature change from 22°C to 27°C.

where 10% of the optical port is extracted to the spectrometer (OSA) and the other port is fed back into the laser cavity.

III. Experimental Results and Discussion

The pre-experiment based on a broadband light source was monitored at room temperature (22°C-27°C). The LC-SHF structure is fixed by two conductive glasses, and the modulator is placed inside the thermostat (CB1701, Biopioneer Tech Co., Ltd, China). Set the temperature interval at 1°C and change the temperature every half an hour. When the temperature is stable and the output laser spectrum no longer drifts, the readings are recorded to ensure the accuracy of the obtained data. Conductive glass side walls are not fully encapsulated to increase the interaction between ambient temperature and LC. The temperature was increased at a step of 1°C each time. At the beginning of the experiment, the ambient temperature of SHF structure was 22°C. Each test was left standing for 45 minutes to ensure the reliability of the results. Fig.6 shows the transmission spectrum of the temperature from 22°C to 27°C. As the temperature rises, the shift of laser peak indicates that the laser peak has a blue shift and the light wavelength moves to a shorter wavelength. According to Equation (5), the shift of laser peak wavelength depends on the change of effective refractive index difference. It shows that the effective refractive index difference decreases with the increase of temperature due to thermo-optic effect. The corresponding spectrum is shown in Fig.7. The test results show that the wavelength is shifted from 1520nm to 1495nm. It shows good linear stability with a sensitivity of 4.79nm/°C, as shown in Fig.8.

Fig. 9 shows the transmission spectrum excursions of the sample from 80 V_{rms} to 104 V_{rms} at 2kHz AC voltage. When an electric field greater than the threshold voltage and perpendicular to the air axis is applied, the LC molecules will overcome the effects of surface anchoring energy and thermal motion and reorient under electric field modulation. In this structure, the threshold voltage of E7 LC is 80V_{rms}, and the resonance wavelength at about 1500 nm in the transmission

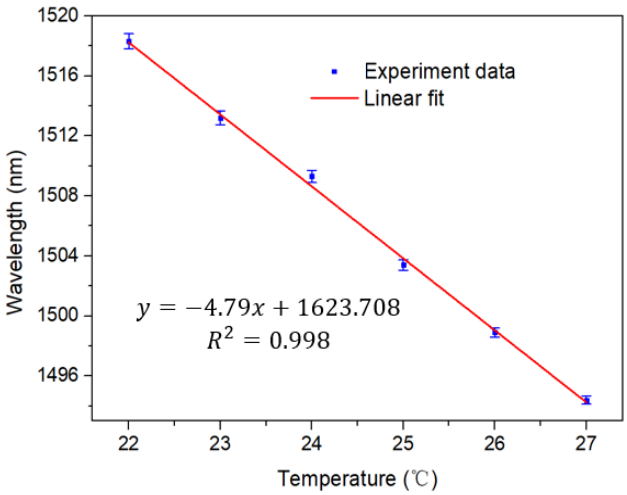

Fig. 8. Function relationship between the temperature and the Interference peaks wavelength with temperature change from 22°C to 27°C.

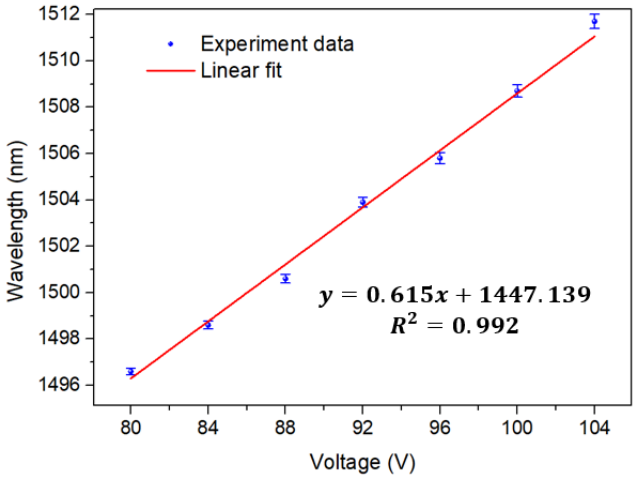

Fig. 10. Function relationship between the electric field and the Interference peaks wavelength with electric field change from 80V_{rms} to 104V_{rms}.

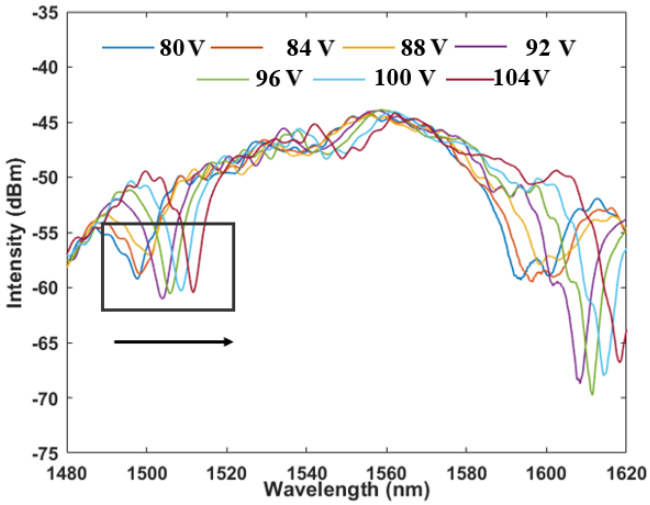

Fig. 9. Transmission spectrum evolution in supercontinuum light source with electric field change from 80V_{rms} to 104V_{rms}.

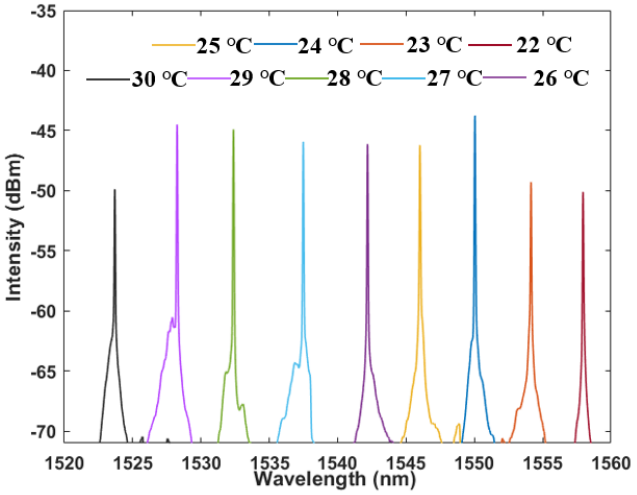

Fig. 11. Transmission spectra of the FRL based temperature modulator when T changes from 22°C to 30°C with the steps of 1°C.

spectrum is red shifted. When the applied voltage exceeds this threshold value, LC molecules in the air hole are arranged regularly in the direction of the electric field, resulting in both regular RI changes and linear wavelength shift. Yang *et al.* [23] described and explained this phenomenon. As shown in Fig. 9, when the applied voltage is further increased from 85 V_{rms} to 104 V_{rms}, the interference peak shifts linearly from 1496nm to 1512nm. The results of linear fitting show that the tuning efficiency of the device is up to 0.615 nm/V_{rms}. These high sensitivity results from the critical phase matching condition between the fiber core mode and the liquid waveguide mode, and the resonant wavelength is determined by the intersection between the dispersion curve of the fiber core mode and the liquid waveguide mode. When the RI of the liquid waveguide changes slightly, such as when the temperature or electric field changes, the resonant wavelength usually shifts greatly. This means that our device has good potential for high sensitivity wavelength demodulation temperature and electric field sensing.

A related point is that upon excitation by the AC voltage source, some power dissipation should occur in the LC filled hole and the temperature should increase (which would lead to a blue shift). The net shift is still towards longer wavelengths so the voltage induced shift competes successfully with the opposite thermally induced one. In this case, the change in the electric field remains linear. This is a good proof that the sensor can still work under the influence of temperature.

Further, the FRL system was used to test the temperature range from 22 °C to 30 °C to investigate the performance of the modulator. The results are shown in Fig. 11 and 12. As is known to all, with the increase of temperature, the effective RI decreases affected by thermo-optic effect. The transmission spectrum of fiber ring laser will shift to shorter wavelength and the emission wavelength will appear blue shift. The detection sensitivity is up to 4.23nm/°C, a five-fold improvement over conventional FRL based temperature sensors. Compared with the broadband light source, the detection sensitivity is slightly lower, which we think may be due to the physical deviation

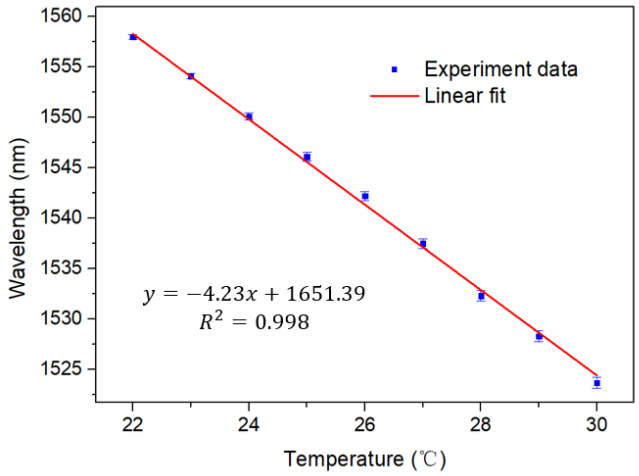

Fig. 12. Variations of the emission wavelength when T changes from 22°C to 30°C with the steps of 1°C.

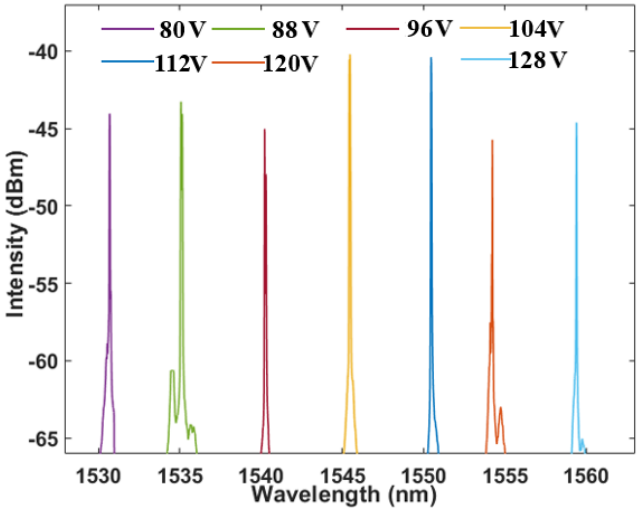

Fig. 13. Transmission spectra of the FRL based electric field modulator when electric field change from 80V_{rms} to 128V_{rms} with the steps of 8V_{rms}.

caused by the interference spectrum clutter after the injection of liquid crystal. However, as shown in Fig. 12, the temperature modulator based on the FRL system still maintains good linearity. Interference peaks also exist between 1525nm-1560nm according to the spectrum of broadband light source. This is within the laser pump gain threshold, so that the peak laser output can be obtained as the external parameters change.

Fig.13 shows the transmission spectrum of the FRL modulator from 80 V_{rms} to 128 V_{rms} at a 2kHz AC voltage. A high SNR (greater than 30dB) and a narrow 3dB bandwidth (less than 0.15nm) can be found in Fig.13. This means that our modulator has good potential for long-range, highly sensitive electric field demodulation. As can be seen from Fig. 14, the detection sensitivity is 0.604 nm/V_{rms}. Good consistency was maintained with the data shown in the pre-experiment in Fig. 9.

An important parameter to judge the performance of an FRL modulator is its stability, which determines the application

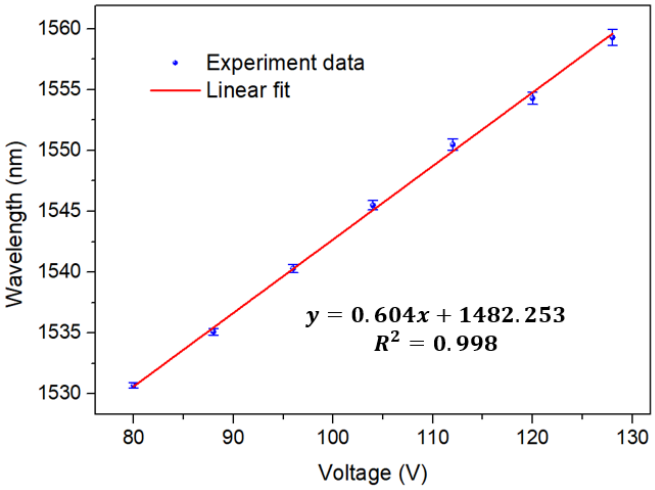

Fig. 14. The fluctuation of the laser output within 5 min at each inclination angle.

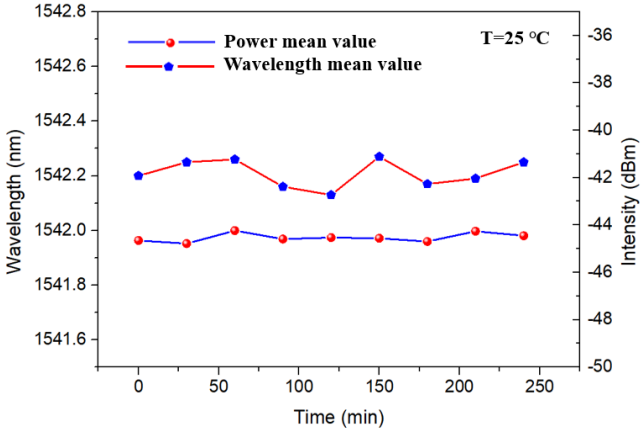

Fig. 15. Test for time stability of wavelength shift and power fluctuation.

TABLE I
SENSITIVITY COMPARISON WITH OTHER TEMPERATURE SENSING STRUCTURES

Structures	Temperature sensitivity(nm /℃)	Eclectic field sensitivity (V_{rms}/℃)	Refs.
Liquid-Filled PCF	1.747	~	[27]
Large mode area fiber	~	0.42	[28]
HCF	~	0.256	[26]
PCF	~	0.53	[25]
SHF	7.38		[29]
PCF+LC	3.9		[30]
This work	4.23	0.604	

field of FRL. The transmitter wavelength and output power of the modulator designed in this experiment were tested for more than 3 hours, as shown in Fig.15. The wavelength difference was less than 0.16nm and the power change was less than 0.1dB, which verified the good performance of the modulator.

The performance of the previously reported work is summarized and compared with our device as shown in Table I.

It can be seen from Table I that the proposed thermo-optic and electro-optic tuner based on LC-SHF modulation has advantages in sensitivity. In addition, the device manufacturing method is very simple, easy to mass production; It can meet most testing requirements.

IV. Conclusion

A SHF ultra-high sensitivity electric field and temperature modulator based on LC penetration in FRL system is proposed and demonstrated experimentally. SHF can form a temperature and electric field modulator under the combined action of the high thermal and photoelectric effect of the liquid crystal and the interference of the core mode and cladding mode in SHF. Based on this, SHF in the system acts as a laser filter and sensor head at the same time. In addition, the LC-Filled PCF has a temperature sensitivity of up to 4.23nm/°C due to the special temperature response of the LC. The sensitivity of electric field modulated by electro-optic effect is 0.604nm/Vrms. Furthermore, the FRL system has a high signal-to-noise ratio (∼30dB), a 3dB band width (less than 0.15nm), and good stability. Therefore, thermo-optic and electro-optic modulator proposed has potential to be applied to remote environmental monitoring and power engineering.

References

[1] Y. Tian *et al.*, "High sensitivity liquid level sensor based on dual side-hole fiber Mach–Zehnder interferometer," *Opt. Commun.*, vol. 440, pp. 194–200, Jun. 2019.

[2] J. Hu *et al.*, "Dual Mach–Zehnder interferometer based on side-hole fiber for high-sensitivity refractive index sensing," *IEEE Photon. J.*, vol. 11, no. 6, pp. 1–13, Dec. 2019.

[3] S. Li and Y. Zhao, "A Mach–Zehnder interferometer based on tapered dual side hole fiber for refractive index sensing," *Opt. Fiber Technol.*, vol. 45, pp. 267–270, Nov. 2018.

[4] X. Zhou, X. Li, S. Li, G.-W. An, and T. Cheng, "Magnetic field sensing based on SPR optical fiber sensor interacting with magnetic fluid," *IEEE Trans. Instrum. Meas.*, vol. 68, no. 1, pp. 234–239, Jan. 2019.

[5] L. De Maria and D. Bartalesi, "A fiber-optic multisensor system for predischarges detection on electrical equipment," *IEEE Sensors J.*, vol. 12, no. 1, pp. 207–212, Jan. 2012.

[6] Q. Wang, L. Zhang, C. Sun, and Q. Yu, "Multiplexed fiber-optic pressure and temperature sensor system for down-hole measurement," *IEEE Sensors J.*, vol. 8, no. 11, pp. 1879–1883, Nov. 2008.

[7] J. Posada-Roman, J. A. Garcia-Souto, and J. Rubio-Serrano, "Fiber optic sensor for acoustic detection of partial discharges in oil-paper insulated electrical systems," *Sensors*, vol. 12, no. 4, pp. 4793–4802, 2012.

[8] Z. Brodzeli *et al.*, "Sensors at your fibre tips: A novel liquid crystal-based photonic transducer for sensing systems," *J. Lightw. Technol.*, vol. 31, no. 17, pp. 2940–2946, Sep. 1, 2013.

[9] J. Du, Y. Liu, Z. Wang, B. Zou, B. Liu, and X. Dong, "Electrically tunable Sagnac filter based on a photonic bandgap fiber with liquid crystal infused," *Opt. Lett.*, vol. 33, no. 19, pp. 2215–2217, Sep. 2008.

[10] E. Reyes-Vera, C. M. B. Cordeiro, and P. Torres, "Highly sensitive temperature sensor using a Sagnac loop interferometer based on a side-hole photonic crystal fiber filled with metal," *Appl. Opt.*, vol. 56, no. 2, pp. 156–162, 2017.

[11] X. Y. Chen *et al.*, "Liquid crystal-embedded tilted fiber grating electric field intensity sensor," *J. Lightw. Technol.*, vol. 35, pp. 3347–3353, Aug. 15, 2017.

[12] Y. Huang *et al.*, "Liquid-crystal-filled side-hole fiber for high-sensitivity temperature and electric field measurement," *Micromachines*, vol. 10, no. 11, p. 761, Nov. 2019.

[13] C. Yang, H. Zhang, B. Liu, S. Lin, Y. Li, and H. Liu, "Electrically tunable whispering gallery mode microresonator based on a grapefruit-microstructured optical fiber infiltrated with nematic liquid crystals," *Opt. Lett.*, vol. 42, no. 15, pp. 2988–2991, 2017.

[14] T. Muñoz-Hernández, E. Reyes-Vera, and P. Torres, "Tunable whispering gallery mode photonic device based on microstructured optical fiber with internal electrodes," *Sci. Rep.*, vol. 9, no. 1, Aug. 2019, Art. no. 12083.

[15] K. Bednarsk *et al.*, "Enhancement of thermal and electro-optical properties of photonic crystal fibers infiltrated with a modified 6CHBT nematic liquid crystal doped with gold nanoparticles," *Opt. Mater.*, vol. 98, pp. 109419–109425, Dec. 2019.

[16] Y. Huang *et al.*, "Tunable electro-optical modulator based on a photonic crystal fiber selectively filled with liquid crystal," *J. Lightw. Technol.*, vol. 37, no. 9, pp. 1903–1908, May 1, 2019.

[17] E. Reyes-Vera and P. Torres, "Influence of filler metal on birefringent optical properties of photonic crystal fiber with integrated electrodes," *J. Opt.*, vol. 18, no. 8, Aug. 2016, Art. no. 085804.

[18] M. Fokine *et al.*, "Integrated fiber Mach–Zehnder interferometer for electro-optic switching," *Opt. Lett.*, vol. 27, no. 18, pp. 1643–1645, 2002.

[19] L. Scolari *et al.*, "Continuously tunable devices based on electrical control of dual-frequency liquid crystal filled photonic bandgap fibers," *Opt. Exp.*, vol. 13, no. 19, pp. 7483–7496, Sep. 2005.

[20] L. Liang, G. Ren, B. Yin, W. Peng, X. Liang, and S. Jian, "Refractive index and temperature sensor based on fiber ring laser with STCS fiber structure," *IEEE Photon. Technol. Lett.*, vol. 26, no. 21, pp. 2201–2204, Nov. 1, 2014.

[21] W. Lin *et al.*, "In-fiber Mach–Zehnder interferometer sensor based on er doped fiber peanut structure in fiber ring laser," *J. Lightw. Technol.*, vol. 39, no. 10, pp. 3350–3357, May 15, 2021.

[22] W. Lin, Y. Liu, L. Shao, and M. I. Vai, "A fiber ring laser sensor with a side polished evanescent enhanced fiber for highly sensitive temperature measurement," *Micromachines*, vol. 12, no. 5, p. 586, May 2021.

[23] W. Lin *et al.*, "Temperature sensor based on fiber ring laser with cascaded fiber optic Sagnac interferometers," *IEEE Photon. J.*, vol. 13, no. 2, pp. 1–12, Apr. 2021.

[24] H. Du, X. Sun, Y. Hu, X. Dong, and J. Zhou, "High sensitive refractive index sensor based on cladding etched photonic crystal fiber Mach–Zehnder interferometer," *Photon. Sensors*, vol. 9, no. 2, pp. 126–134, Jun. 2019.

[25] S. Tian *et al.*, "Multi-band thermal optical switch based on nematic liquid crystal filled photonic crystal fiber," *J. Lightw. Technol.*, vol. 39, no. 10, pp. 3297–3302, May 15, 2021.

[26] Y. Liu, C. Zhao, Y.-N. Zhang, G. Ma, X. Li, and Y. Zhao, "Electrically tunable optical fiber device based on hollow-core fiber infiltrated with liquid crystal," *Sens. Actuators A, Phys.*, vol. 318, Feb. 2021, Art. no. 112500.

[27] X. Yang, Y. Lu, B. Liu, and J. Yao, "Fiber ring laser temperature sensor based on liquid-filled photonic crystal fiber," *IEEE Sensors. J.*, vol. 17, no. 21, pp. 6948–6952, Nov. 2017.

[28] L. Wei, L. Eskildsen, J. Weirich, L. Scolari, T. T. Alkeskjold, and A. Bjarklev, "Continuously tunable all-in-fiber devices based on thermal and electrical control of negative dielectric anisotropy liquid crystal photonic bandgap fibers," *Appl. Opt.*, vol. 48, no. 3, pp. 497–503, Jan. 2009.

[29] B. H. Kim, S. H. Lee, D. H. Son, T. J. Ahn, S. E. Kim, and W. T. Han, "Optical properties of the fiber-optic temperature sensor based on the side-hole fiber filled with indium," *Appl. Opt.*, vol. 52, no. 4, pp. 666–673, Feb. 2013.

[30] D. J. J. Hu *et al.*, "Fabrication and characterization of a highly temperature sensitive device based on nematic liquid crystal-filled photonic crystal fiber," *IEEE Photon. J.*, vol. 4, no. 5, pp. 1248–1255, Oct. 2012.

Weihao Lin received the B.Eng. degree in optoelectronic information science and engineering from the Southern University of Science and Technology, China, in 2019. He is currently pursuing the Ph.D. degree under a collaboration program between the Southern University of Science and Technology and the University of Macau. His research interests include optical fiber sensor, fiber laser sensors, and fiber lasers.

Siming Sun received the B.Eng. degree in optoelectronic information science and engineering from the Huazhong University of Science and Technology, China, in 2020.

Li-Yang Shao (Senior Member, IEEE) received the Ph.D. degree in optical engineering from Zhejiang University, China, in 2008. From 2006 to 2009, he was with The Hong Kong Polytechnic University as a Research Assistant/Associate, working on fiber grating devices and sensors. Then, he was a Postdoctoral Fellow with the Department of Electronics, Carleton University, Canada. In 2011, he returned to The Hong Kong Polytechnic University for another Postdoctoral Research Project. In 2012, he was granted the Endeavor Research Fellowship from the Australian Government and working with the Interdisciplinary Photonics Laboratory, The University of Sydney. In 2013, he joined Southwest Jiaotong University as a Full Professor. In 2017, he joined the Department of Electrical and Electronic Engineering, Southern University of Science and Technology. In 2018, he became the Associate Dean with the School of Innovation and Entrepreneurship, Southern University of Science and Technology. He has authored/coauthored more than 150 articles in the refereed international journals/conferences with a total citation of more than 2800 times (SCI citation of over 1800 times by the other researchers). His research interests include fiber grating and sensors, distributed fiber optic sensing, microwave photonics for sensing, and smart sensing systems for railway industry. He acts as the Principal Investigator for several high-level projects, such as NSFC projects, International Science and Technology Cooperation Program of China, etc. He was a TPC or Organizing Committee Member of multiple conferences, including ICAIT 2009–2013, PGC 2010, OFS 2011, PIERS 2014, ICOCN 2015–2016, PGC 2017, APOS 2018, CLEO-PR 2018, ACP 2019, APOS 2019, and CLEO-PR 2020. He serves as a Reviewer for more than 20 SCI journals, including *Optics Letters*, *Optics Express*, the *Journal of Lightwave Technology*, and the IEEE PHOTONICS TECHNOLOGY LETTERS.

Mang I. Vai (Senior Member, IEEE) received the Ph.D. degree in electrical and electronics engineering from the University of Macau, China, in 2002.

He is currently a Coordinator with the State Key Laboratory of Analog and Mixed-Signal VLSI and an Associate Professor of Electrical and Computer Engineering with the Faculty of Science and Technology, University of Macau. Since 1984, he has been performing research in the areas of digital signal processing and embedded systems.

Perry Ping Shum (Senior Member, IEEE) received the B.Eng. and Ph.D. degrees in electronic and electrical engineering from the University of Birmingham, Birmingham, U.K., in 1991 and 1995, respectively. In 1999, he joined the School of Electrical and Electronic Engineering, Nanyang Technological University, Nanyang, China. He has authored or coauthored more than 400 international journals and conference papers. His research interests are concerned with optical communications, fiber sensors, and fiber lasers. He is the technical program chair, a committee member, and the international advisor of many international conferences.

Yuhui Liu received the B.Eng. degree in optoelectronic information science and engineering from the Southern University of Science and Technology, China, in 2019. She is currently pursuing the Ph.D. degree under a collaboration program between the Southern University of Science and Technology and The Hong Kong Polytechnic University.

Weizhi Wang received the M.S. degree in information and communication engineering from the Harbin Institute of Technology, Shenzhen, China, in 2011. He is now an Engineer with the Peng Cheng Laboratory, Shenzhen.